RSC Mechanochemistry

ROYAL SOCIETY OF CHEMISTRY

PAPER

View Article Online
View Journal | View Issue

Cite this: *RSC Mechanochem.*, 2025, **2**, 116

Mechanochemical ZIF-9 formation: *in situ* analysis and photocatalytic enhancement evaluation†

Noelia Rodríguez-Sánchez, [ab] Carsten Prinz,[a] Ralf Bienert, [a] Menta Ballesteros, [bc] A. Rabdel Ruiz Salvador, [bd] Biswajit Bhattacharya *[a] and Franziska Emmerling *[ae]

Received 2nd October 2024
Accepted 18th November 2024

DOI: 10.1039/d4mr00114a

rsc.li/RSCMechanochem

Efficient treatment of persistent pollutants in wastewater is crucial for sustainable water management and environmental protection. This study addresses this challenge by investigating the mechanochemical synthesis and photocatalytic performance of ZIF-9, a cobalt-based zeolitic imidazolate framework. Using synchrotron-based powder X-ray diffraction, we provide real-time insights into the formation dynamics of ZIF-9 during mechanosynthesis. Our results show that mechanochemically synthesised ZIF-9 exhibits superior photocatalytic activity compared to its solvothermally prepared counterpart, achieving a 2-fold increase in methylene blue degradation rate. This research not only advances our understanding of the synthesis and properties of ZIF-9, but also demonstrates the potential of mechanochemical approaches in the development of high-performance, sustainably produced materials for water treatment and other environmental applications.

Introduction

Access to clean water and its sustainable management are critical challenges facing contemporary society, particularly amid increasing scarcity and contamination of water resources. Reuse of treated wastewater in agriculture,[1] industry,[2] and urban supply[3] offers a viable strategy to mitigate the global water crisis. However, this requires the effective removal of recalcitrant contaminants, such as pharmaceuticals,[4] personal care products,[5] and hazardous industrial chemicals[6] among others.[7]

Advanced Oxidation Processes (AOPs) have attracted attention in recent years for their effectiveness in degrading pollutants. Among them, photocatalytic reactions stand out due to their potential for complete mineralization of contaminants, through the generation of reactive species, under light irradiation that break down complex organic molecules.[8] The photo-Fenton process, based on the addition of H_2O_2, has received much attention as one of the most studied photocatalytic AOPs in water treatment, and has traditionally been conducted using homogeneous catalysts like iron salts under light exposure.[9,10] However, it has limitations related to the homogeneous nature of the catalyst, such as difficulties in catalyst recovery and the generation of iron sludge.[11] In contrast, heterogeneous photo-Fenton processes, using metal ions immobilized on solid catalysts, offer advantages in recovery and reuse, reducing leaching and thus, secondary pollution.[12] In this context, metal–organic frameworks (MOFs) have emerged as promising materials in heterogeneous photo-Fenton processes, due to their high surface area, tunable porosity, and structural versatility.[13,14] These materials can encapsulate active sites within their frameworks, enhancing pollutant degradation and improving catalyst stability and reusability.[15,16] However, their widespread industrial application has been limited by the high costs and environmental drawbacks associated with conventional synthesis methods.[17,18] They typically involve dissolving precursors in a solvent and heating them under specific pressure and temperature conditions and often require lengthy reaction times, high energy consumption, and the use of toxic solvents, which pose significant economic challenges and environmental and safety concerns.[19] As a result, there is an urgent need for more sustainable and efficient synthesis methods, in line with the principles of green chemistry.[20–22]

Mechanochemical synthesis has demonstrated significant advantages, including rapid reaction times, the ability to use insoluble metal sources and the use of solvent-free or solvent-minimal approaches,[22] which significantly reduces the environmental footprint and safety hazards associated with

[a]*BAM Federal Institute for Materials Research and Testing, Richard-Willstätter-Straße 11, 12489, Berlin, Germany. E-mail: biswajit.bhattacharya@bam.de; franziska.emmerling@bam.de*

[b]*Center for Nanoscience and Sustainable Technologies (CNATS), Universidad Pablo de Olavide, Ctra. Utrera km. 1, 41013, Seville, Spain*

[c]*Department of Molecular Biology and Biochemistry Engineering, Universidad Pablo de Olavide, Ctra. Utrera km. 1, 41013, Seville, Spain*

[d]*Department of Physical, Chemical and Natural Systems, Universidad Pablo de Olavide, Ctra. Utrera km. 1, 41013, Seville, Spain*

[e]*Department of Chemistry, Humboldt-Universität of Berlin, Brook-Taylor-Strasse 2, 12489 Berlin, Germany*

† Electronic supplementary information (ESI) available. See DOI: https://doi.org/10.1039/d4mr00114a

traditional methods.[23,24] Additionally, mechanochemical synthesis is typically faster and can be conducted at ambient temperature and pressure, making it more energy-efficient.[25,26] Moreover, mechanochemical reactions can be understood by observing and analyzing them through time resolved *in situ* monitoring (TRIS).[27,28] By providing continuous, real-time data, this technique allows detailed insights into reaction mechanisms, kinetics and intermediates formed during the process.[27,29] This real-time monitoring uses analytics such as *in situ* synchrotron-based powder X-ray diffraction (PXRD), Raman spectroscopy, and infrared (IR) spectroscopy or combinations thereof, integrated directly into the mechanochemical setup.[23,30] The advantage of *in situ* characterisation is its ability to provide integral information on the evolution of the material, allowing real-time optimisation of reaction conditions and improved reproducibility.[27,31]

In the last decade, different functional materials, including MOFs, have been synthesized using mechanochemical methods, offering a more sustainable and efficient alternative to conventional approaches.[24,32–34] However, while it is well known that crystallisation can occur rapidly under mechanical treatment,[35,36] the potential impact of this treatment on the physico-chemical properties of the material remains uncertain. This gap in understanding has prompted us to explore how different synthesis methods influence the photocatalytic properties of ZIF-9, which is a member of the zeolitic imidazolate framework (ZIF) family. ZIF-9 has been widely studied for catalytic processes, such as the oxygenation of aromatic compounds and hydrogen production.[37] Specifically, we aim to optimize the synthesis conditions and achieve a reproducible mechanochemical ZIF-9 with well-defined structural properties, including the first-ever *in situ* monitoring investigation of ZIF-9. Finally, to elucidate how these methodologies affect its functional properties, we have evaluated and compared the effects of solvothermal and mechanochemical synthesis on the photocatalytic performance of this MOF by the degradation of methylene blue (MB) through heterogeneous photo-Fenton process under visible light.

Materials and methods

Materials

Cobalt nitrate hexahydrate ($Co(NO_3)_2 \cdot 6H_2O$, ≥99%) and ammonium sulfate ($(NH_4)_2SO_4$, ≥99.5%) were purchased from ACS reagents. Benzimidazole (bIm, ≥99%), Cobalt(II) hydroxide ($Co(OH)_2$, ≥95%) and methylene blue were obtained from Sigma Aldrich. Ammonium chloride (NH_4Cl, ≥99%) was purchased from Fisher Scientific. Ethanol absolute, methanol, hydrogen peroxide, *N*,*N*-dimethylformamide, ammonium nitrate (NH_4NO_3, ≥99%) and ammonium hydroxide 25% (NH_4OH) were acquired from ChemSolute.

Characterization of ZIF-9

ZIF-9 was characterized by X-ray diffraction (XRD) using a Bruker D8 Advance X-ray diffractometer. The Fourier transform infrared (FTIR) spectroscopy measurements were performed using a Thermo Nicolet NEXUS 470 FTIR spectrophotometer and TGA thermogravimetry was conducted to study the thermal stability of the samples using a Thermal Analysis System TGA/DSC 3+ equipment under N_2 atmosphere. Scanning Electron Microscopy (SEM) was carried out under a XL30 ESEM. Transmission Electron Microscopy (TEM) images were obtained using a Talos F200S microscope (Thermo Fisher Scientific). A Ceta 16M camera (TEM mode) and a HAADF and BF detector (STEM mode; Scanning Transmission Electron Microscopy) were used to capture the images. A Super-X G2 detector equipped with two silicon drift detectors (SDD) was used during the TEM analysis for Energy Dispersive X-ray Spectroscopy (EDS) to determine the elemental composition of the samples. BET analyses were performed under ASAP from the Micromeritics Instrument Corporation company and the isotherms were measured with nitrogen at 77 K. The specific surface areas ABET were hereby calculated in a relative pressure range between $0.04 \leq p/p_0 < 0.22$ of the isotherms using the multipoint method of Brunauer, Emmett and Teller (BET) with a minimum of five supporting points. *In situ* X-ray diffraction monitoring was carried out on the μSpot beamline (BESSY II, Helmholtz Centre Berlin for Materials and Energy), using a beam diameter of 100 μm at a photon flux of $1 \times 109\ s^{-1}$ at a ring current of 100 mA. Scattered intensities were collected with a two-dimensional X-ray detector (MarMosaic, CCD 3072 × 3072) and a time-resolution of 15 s. A Shimazdu UC-1900i UV-vis spectrophotometer was used to determine absorbance during the decontamination tests.

Synthesis of ZIF-9

Solvothermal synthesis of ZIF-9. Solvothermal synthesis of ZIF-9 was carried out according to Park *et al.*, 2006 with a slight modification. For ZIF-9, 1 mM of bIm (0.120 g) and 1.4 mM of cobalt nitrate hexahydrate $Co(NO_3)_2 \cdot 6H_2O$ (0.420 g) were dissolved in 36 mL of dimethylformamide (DMF) stirring at room temperature. The mixture was then poured into a hydrothermal autoclave and placed in an oven at 5 °C min^{-1} to 130 °C for 48 h, and cooling at 0.4 °C min^{-1}. The samples were centrifuged and washed three times with DMF (3 mL × 3) and let dry at room temperature. Finally, it was placed in a vacuum dryer at 100 °C for 24 h. The final molar ratio used for the synthesis was 1 : 1.4 : 465 for the reagents bIm : $Co(NO_3)_2 \cdot 6H_2O$: DMF.

Mechanochemical synthesis of ZIF-9. Several additives (NH_4Cl, NH_4NO_3, NH_4OH, and $(NH_4)_2SO_4$) and solvents (water, methanol, ethanol and DMF) were evaluated as coadditives to optimize the synthesis of mechanochemical ZIF-9. The amount of additive was 20 mg, except for NH_4NO_3 which was 13 mg, while 200 μL of solvent was used. The highly optimized synthesis of mechanochemical ZIF-9 was achieved by mixing 1 mM of bIm (0.120 g), 0.5 mM of cobalt(II) hydroxide (0.046 g) and 0.09 mM of NH_4Cl (5 mg) with 40 μL of DMF in a 10 mL stainless steel jar with a 9 mm stainless steel ball for horizontal ball milling and an 8 mm stainless steel ball for vertical ball milling. The mixture was milled for 50 minutes at a rate of 30 Hz using a Retsch MM400 shaker-type mixer mill and at 50 Hz using a Fritsch Pulverisette 23 for vertical milling, as

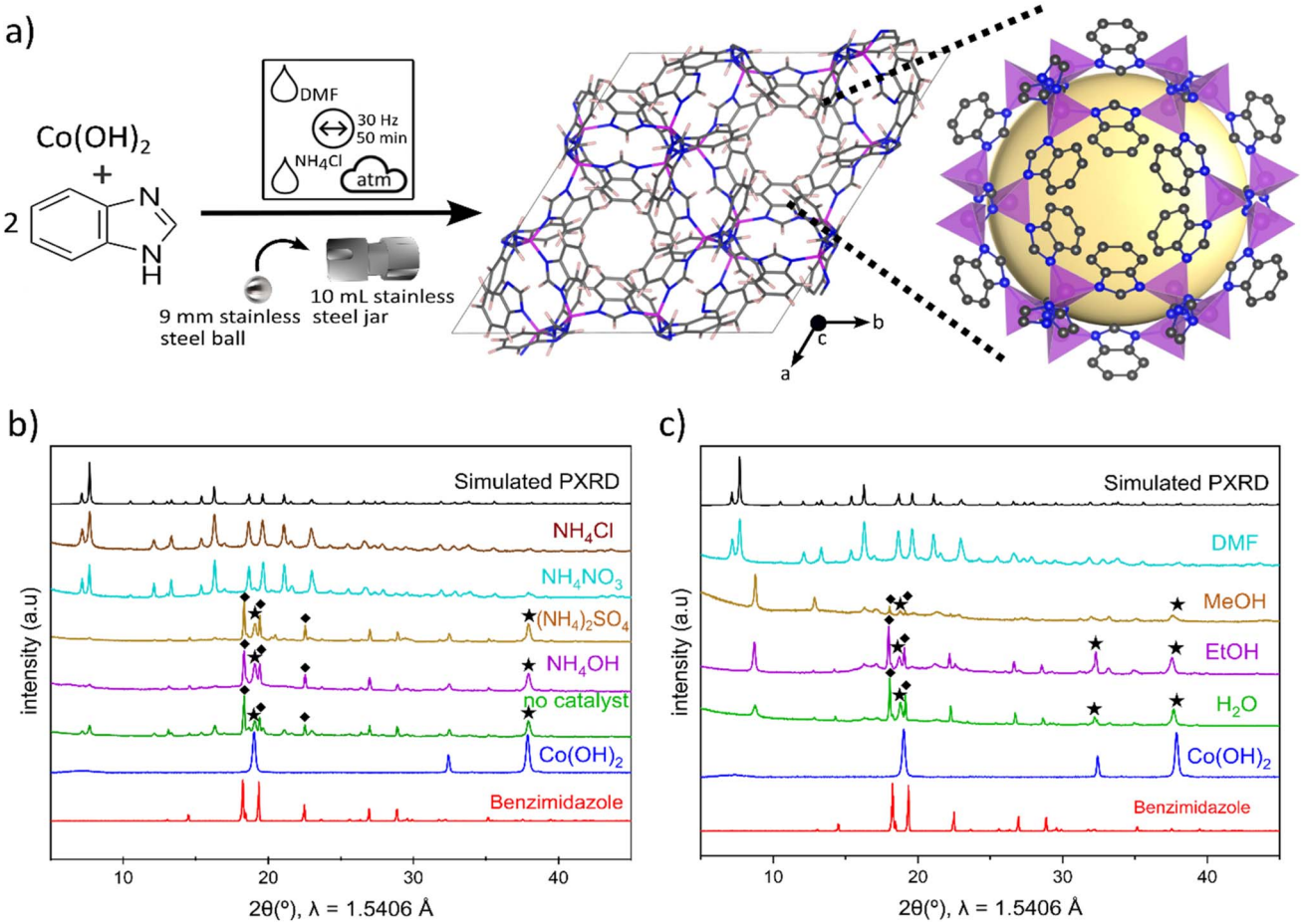

Fig. 1 Schematic representation of the mechanochemical synthesis using horizontal ball milling (a), PXRD patterns for mechanochemical ZIF-9 according to the additive used. Mechanochemical reactions symbols were represented according to Michalchuk *et al.*[38] (b) and according to the solvents using NH_4Cl as additive (c), being $Co(OH)_2$ peaks represented by stars (★) benzimidazole represented by rhombuses (◆).

schematically shown in Fig. 1. The powder was collected scratching the wall of the jar. Finally, the MOF was washed three times with DMF (3 mL) and dried at room temperature. The final molar ratio used for the synthesis was 1 : 0.5 : 0.09 : 0.5 for the reagents bIm : $Co(OH)_2$: NH_4Cl : DMF.

For *in situ* characterization, the mechanochemical synthesis of ZIF-9 was carried out using the same procedure and optimized conditions applied under vertical ball milling but using a custom-designed 2.3 mL PMMA jar consisting in a transparent Persplex center piece of 0.75 mm thickness and two stainless steel pieces as caps, thus allowing the incidence of X-rays on the sample.

Photo-Fenton and stability experiments

A 50 mL reactor was placed under a 24 W visible lamp and on a magnetic stirrer at 800 rpm. The reactor was covered to ensure maximum light incidence. The reactor was connected by a cooling tube to a water bath, which was also connected to a temperature controller to keep it at 25 °C.

To evaluate the photocatalytic properties of the solvothermal and mechanochemical ZIF-9, a MB solution (50 mL, 5 mg L^{-1}) and 0.5 g L^{-1} of the catalyst were added to the photoreactor and left in the dark for 60 minutes, stirring at 800 rpm and a temperature of 25 °C. This allows the adsorption of MB on the MOF to be measured until equilibrium is reached. H_2O_2 was then added to reach an initial concentration of 10 mM (35 μL). The light was activated, and irradiation was maintained in the reactor for 165 min. Samples were taken every 15 minutes, centrifuged and their absorbance was measured using a UV/Vis spectrophotometer at 664 nm. To avoid loss of catalyst or solution volume and ensure accuracy of results, all samples were returned to the reactor. All experiments were repeated 3 times to ensure reproducibility.

After photo-Fenton catalysis test, the ZIFs were recovered by centrifuging the final solution and let them dry in an oven for 2 h at 50 °C. After that, an XRD spectroscopy analysis was carried out to check the structural stability of the ZIF. The recovered mechanochemical synthetized ZIF-9 was used over three consecutive cycles to ensure the recyclability of the ZIF.

Kinetic study of photo-Fenton process

Photo-Fenton test kinetics were primarily analyzed using a first-order kinetic model of Langmuir–Hinshelwood (L–H), as this model is effectively accounts for both the adsorption of MB and

the catalytic degradation under photo-Fenton conditions. This model can be described by the following equation (eqn (1)):[39]

$$r = -\frac{dC}{dt} = \frac{k_{cat} \cdot K \cdot C}{1 + K \cdot C} \quad (1)$$

where r is the reaction rate, k_{cat} is the catalytic rate constant, K is the adsorption equilibrium constant, and C is the concentration of the reactant. On the assumption that due to the low concentration of MB in the tests (5 mg L^{-1}), the term $K \cdot C$ is sufficiently small, such that $1 + K \cdot C \approx 1$, the reaction rate can be approximated as (eqn (2)):

$$r \approx k_{cat} \cdot K \cdot C = k\text{app} \cdot C \quad (2)$$

where k_{app} is the apparent first-order rate constant. Integration of this equation reduces the L–H expression and yields a linear relationship between the natural logarithm of concentration and time (eqn (3)). This approximation, provide a reliable description of the reaction kinetics while allowing for a simpler mathematical treatment.

$$-\ln \frac{[c]}{[c]_0} = k_1 t \quad (3)$$

where [c] is the concentration of each point, [c_0] is the initial concentration, k is the value of the velocity constant and t is the time.

Photo-Fenton test data were also fitted to zero-order and pseudo-second-order kinetic models [eqn (4) and (5)], included in the ESI† for comparison.

$$C_0 - C_t = K_o \times t \quad (4)$$

$$\frac{1}{C_t} = k_2 \times t \quad (5)$$

Langmuir, Freundlich, and Temkin desorption kinetics models[40,41] were also evaluated for mechanochemical synthetized ZIF-9 during dark period. The details can be found on the ESI.†

Results and discussion

ZIF-9 was synthesized by solvothermal and mechanochemical routes and characterized using several techniques to compare both materials. The mechanochemical synthesis was optimized through the addition of different additives and solvents (Fig. 1). Powder X-ray diffraction (PXRD) investigations reveal a material with high crystallinity (Fig. S1†). The intensity and position of the reflections match with those of the solvothermal synthesized ZIF-9 corroborating a high crystallinity of the sample in agreement with the simulated PXRD.[42] In the absence of additives or in presence of NH_4OH or $(NH_4)_2SO_4$ (Fig. 1b) as additive, the transformation to ZIF-9 was incomplete. Reflections observed at 18.3°, 19.4° and 22.5° correspond to benzimidazole, while those at 19° and 37.9° are associated with $Co(OH)_2$, indicating that the staring materials have not been fully reacted. In contrast, the use of NH_4NO_3 or NH_4Cl as additives leads to the successful synthesis of ZIF-9. However, the explosive nature of NH_4NO_3 prevents it from being used on a large scale and therefore this additive cannot be used for the synthesis of ZIF-9 on a large scale. Additionally, it was observed that when using NH_4NO_3 as an additive, the amount required for the synthesis cannot be less than 80 μL of DMF solvent and 13 mg (0.16 mmol) of the additive. However, the optimal synthesis conditions for high crystalline ZIF-9 were attained using only 5 mg (0.09 mmol) of NH_4Cl as the additive and 40 μL of DMF as solvent (Fig. S2 and S3†). No reflection from NH_4Cl could be identified in the structure after synthesis due to its coincident re-reflection at 32° and the low amount of additive used.[35] Also, under optimal conditions, complete incorporation of the starting materials was not achieved with any organic solvents other than DMF (Fig. 1c), underscoring the reaction's dependence on both solvent and additive. Under these optimized conditions, mechanochemical synthesis of ZIF-9 was successfully reproducible using both vertical and horizontal movement shaker mill (Fig. S4†), and was scaled up to 2.3 g, maintaining high crystallinity (Fig. S5†).

The FTIR spectra of mechanochemical ZIF-9 display the characteristic absorption bands of the ZIF-9 framework, albeit with slightly lower intensity compared to its solvothermal counterpart (Fig. 2a). This suggests that while the mechanochemical method may introduce some structural defects, the overall integrity of the framework is largely preserved. The highest intensity bands are identified with the C–C single bonds at 1236 cm^{-1}, C=C at 1459 cm^{-1} characteristic of the aromatic rings of the benzimidazole ligand, followed by the C–N bond at 1297 cm^{-1} and C–H at 736 cm^{-1}. It is also possible to identify the C–C–C bond at 652 cm^{-1}, characteristic of ZIF-9.[43] The presence of all key functional groups in the FTIR spectrum confirms that the mechanochemical approach effectively produces the desired ZIF-9 structure. TGA analysis of both mechanochemical and solvothermal ZIF-9 confirm high thermal stability (Fig. 2b), demonstrating stability up to approximately 500 °C, consistent with previous reports.[42,43] The significant weight loss observed in the thermogram of mechanochemical ZIF-9 is attributed to the presence of low amount of DMF molecules in the framework. The nitrogen adsorption isotherms ZIF-9 from both synthesis methods, measured at 77 K, are presented in Fig. S6†. Similar to previous reports, solvothermal synthesized ZIF-9 exhibit a typical Type I isotherm, characteristic of microporous materials, with a steep rise at low relative pressures and an adsorption capacity nearing 70 cm^3 g^{-1} (STP).[44–46] Whereas, mechanochemically synthesized ZIF-9 shows a typical Type IV isotherm characteristic of a mesoporous system and a adsorption capacity around 50 cm^3 g^{-1} (STP), possibly due to structural defects, how it occurs typically during the use of mechanical forces.[47] BET surface area of solvothermal ZIF-9 was similar to other previous studies,[48,49] being 274.06 m^2 g^{-1} for N_2 adsorption at 77 K, and 10.93 m^2 g^{-1} for mechanochemical ZIF-9 (Table S1†).

SEM and TEM images provide a clear depiction of differences in particle size and morphology of mechanochemically synthesized ZIF-9 and its solvothermal counterpart (Fig. 3). The SEM image of solvothermal ZIF-9 illustrates the formation of large, well-defined, and faceted crystals (Fig. 3c), suggesting that

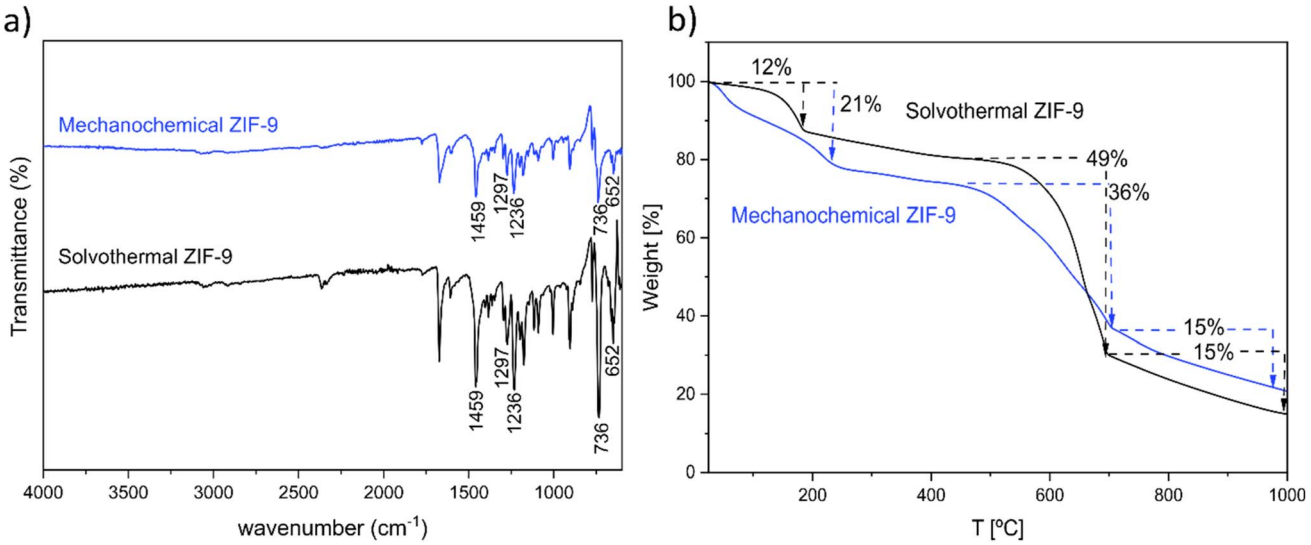

Fig. 2 FTIR spectra for solvothermal synthetized ZIF-9 (black) and mechanochemical synthetized ZIF-9 (blue) (a) and TGA spectra for solvothermal synthesized ZIF-9 (black) and mechanochemical synthetized ZIF-9 (blue) (b).

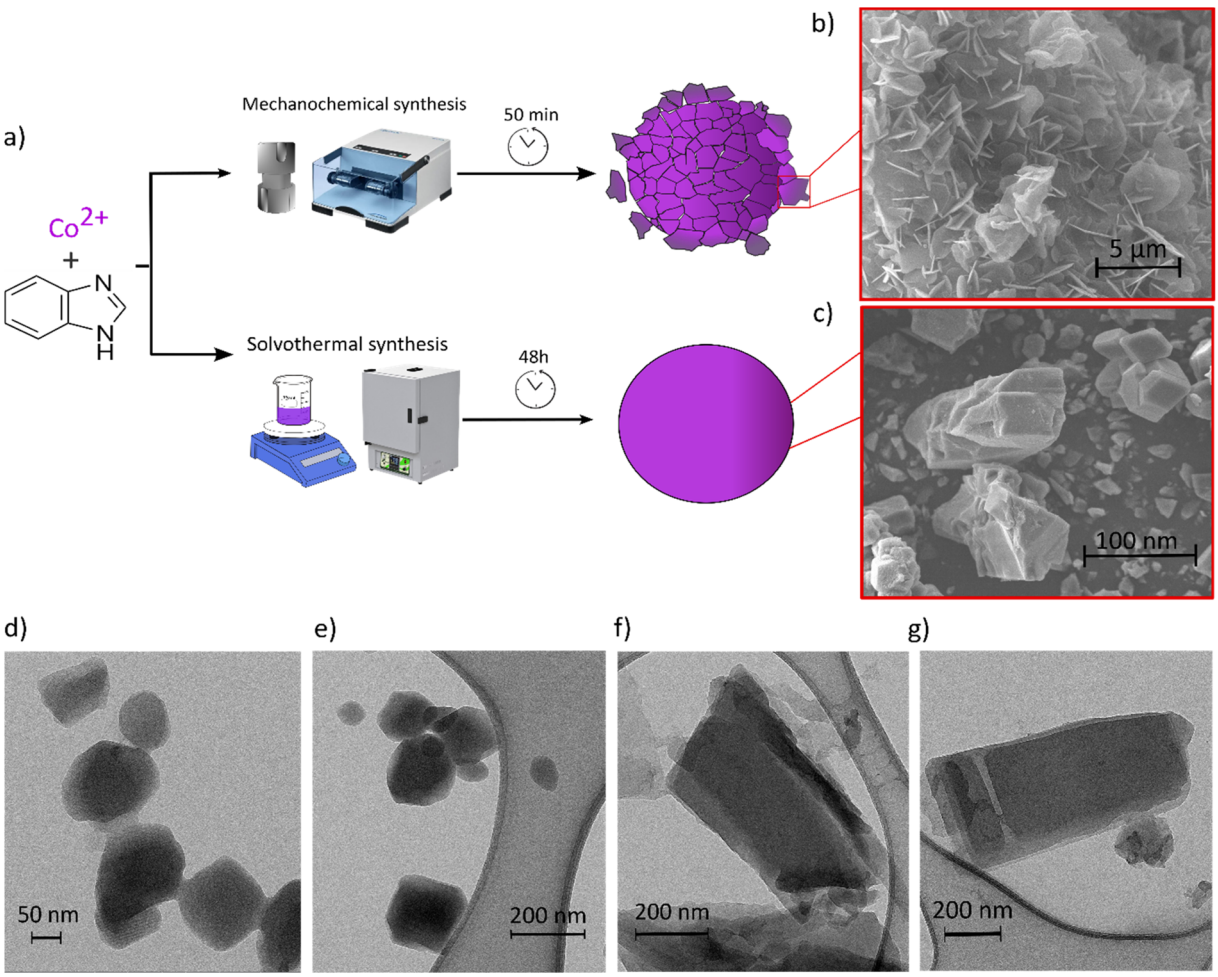

Fig. 3 Schematic d of the synthesis and differences in the surface area of ZIF-9 by mechanochemical and solvothermal synthesis (a), SEM images for mechanochemical ZIF-9 (b) and solvothermal ZIF-9 (c), and TEM images for mechanochemical ZIF-9 (d and e) and solvothermal ZIF-9 (f and g).

the solvothermal process promotes the growth of highly ordered crystalline structures due to the slow and controlled crystallization conditions.[50] This is further supported by TEM images (Fig. 3f and g), which display a high degree of internal order with uniform electron transparency, indicating fewer defects and particle size around 600 nm. In contrast, SEM image of the mechanochemically synthesized ZIF-9 (Fig. 3b) reveals significantly smaller particles with irregular plate-like shapes. TEM analysis (Fig. 3d and e) confirms reduced particle sizes, around 150 nm, and increased surface area, characteristic of the high-energy milling process in mechanochemistry.[51,52] (Fig. 3a). The TEM images of mechanochemical ZIF-9 also show varying degrees of opacity, indicating a more complex internal structure with potential areas of disorder and defects (Fig. 3d and e).[53] In addition, a similar qualitative distribution between solvothermal and mechanochemical ZIF-9 particles was determined by EDS (Fig. S7†).

High-resolution synchrotron-based powder X-ray diffraction data were collected as a function of milling time for ZIF-9 to study the real-time reactions pathway by analyzing the phase composition and crystallinity of intermediates and products (Fig. 4). During the initial phase of grinding, series of peaks corresponding to $Co(OH)_2$ and the benzimidazole ligand are observed. After 15 minutes of grinding, the two characteristic peaks of ZIF-9 appeared at 5.03q/nm^{-1} and 5.39q/nm^{-1}. Around the 35 minutes, new diffraction peaks begin to appear, coinciding with a decrease in intensity of the initial benzimidazole

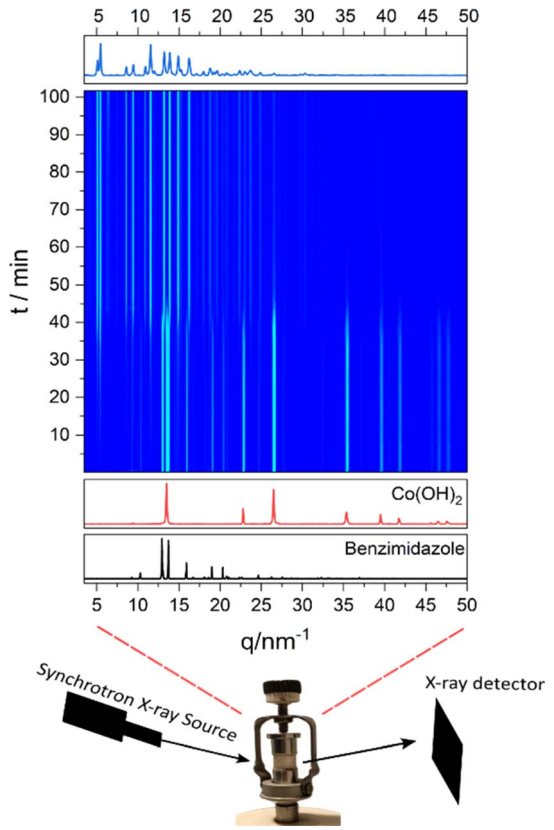

Fig. 4 Time-resolved *in situ* X-ray diffraction data obtained during the mechanochemical synthesis of ZIF-9.

and $Co(OH)_2$ related peaks. This shift is indicative of the formation of ZIF-9 as the reaction progresses towards the assembly of the final MOF structure, finishing after 50 minutes. No peaks belonging to the starting materials are observed, demonstrating pure phase formation. Hence, the above *in situ* investigation reveals that mechanochemical synthesis of ZIF-9 occurs *via* direct transformation from starting materials to ZIF-9, without the formation of any intermediates.

Considering the established linear relationship between decreasing particle size and increasing photocatalytic activity in solid catalysts, as reported in the literature,[54] we observed a significant difference in the particle size of ZIF-9 synthesized *via* mechanochemical and hydrothermal methods (Fig. 3). This prompted us to investigate the photocatalytic properties of both materials in heterogeneous photo-Fenton test. To ensure that the observed effects in the photocatalysis assays are due to photocatalytic activity, a series of control experiments were conducted to measure the contributions of photolysis and the effect of visible light combined with hydrogen peroxide in the absence of the catalysts (Fig. S8†). Visible light contributed to 25% degradation of MB after 165 minutes, attributed to the oxidized form of MB absorbing light in the visible region and initiating photochemical reactions from singlet or triplet excited states (^{1}D*, ^{3}D*).[55–57] On the other hand, the addition of H_2O_2 led to a modest increase in MB degradation, attributed to hydroxyl radicals generated from H_2O_2 under irradiation. Adsorption was then evaluated over 60 minutes in dark conditions to ensure stabilization between the MOF and the contaminant (Fig. 5a). Mechanochemical ZIF-9 adsorbed approximately 20% of MB, consistent with its increased surface area, resulting in a significantly higher concentration of the contaminant on the surface compared to solvothermal ZIF-9. Adsorption isotherms models were evaluated based on Langmuir, Freundlich and Temkin models with a high correlation (Fig. S9, Table S2†). These finding align with the results of Taheri *et al.*, 2020, where the mechanochemical ZIF-8 adsorbed 29.1% of MB and 93.9% of rhodamine B (RhB), while its solvothermal counterpart adsorbed only 3.3% of MB and 41.6% of RhB after 2 hours in dark.[58] We need to consider that since the size of the MB molecules is notoriously higher than the pore delimiting windows of ZIF-9, albeit its flexibility, it is then expected that the observed molecular capture occurs in the external surface. The low particle size of mechanochemically synthesized ZIF-9, provides more active sites for the adsorption of reactants and subsequent photocatalytic reactions.[54,59] We should note that particle size can be also a factor in favoring external surface area, once smaller particles have higher surface volume ratios.[52] As a result, the degradation of the pollutant by mechanochemical ZIF-9 was significantly higher than that by the solvothermal method (Fig. 5a).

Solvothermal synthetized ZIF-9 exhibited low photocatalytic activity, with only a slight decrease in MB concentration over time, achieving 50% of MB degradation. This suggests that solvothermal ZIF-9 lacks significant photocatalytic properties under the experimental conditions. In contrast, mechanochemical ZIF-9 demonstrated a first-order kinetics constant twice as high, with values of 0.0061 min^{-1} for solvothermal ZIF-

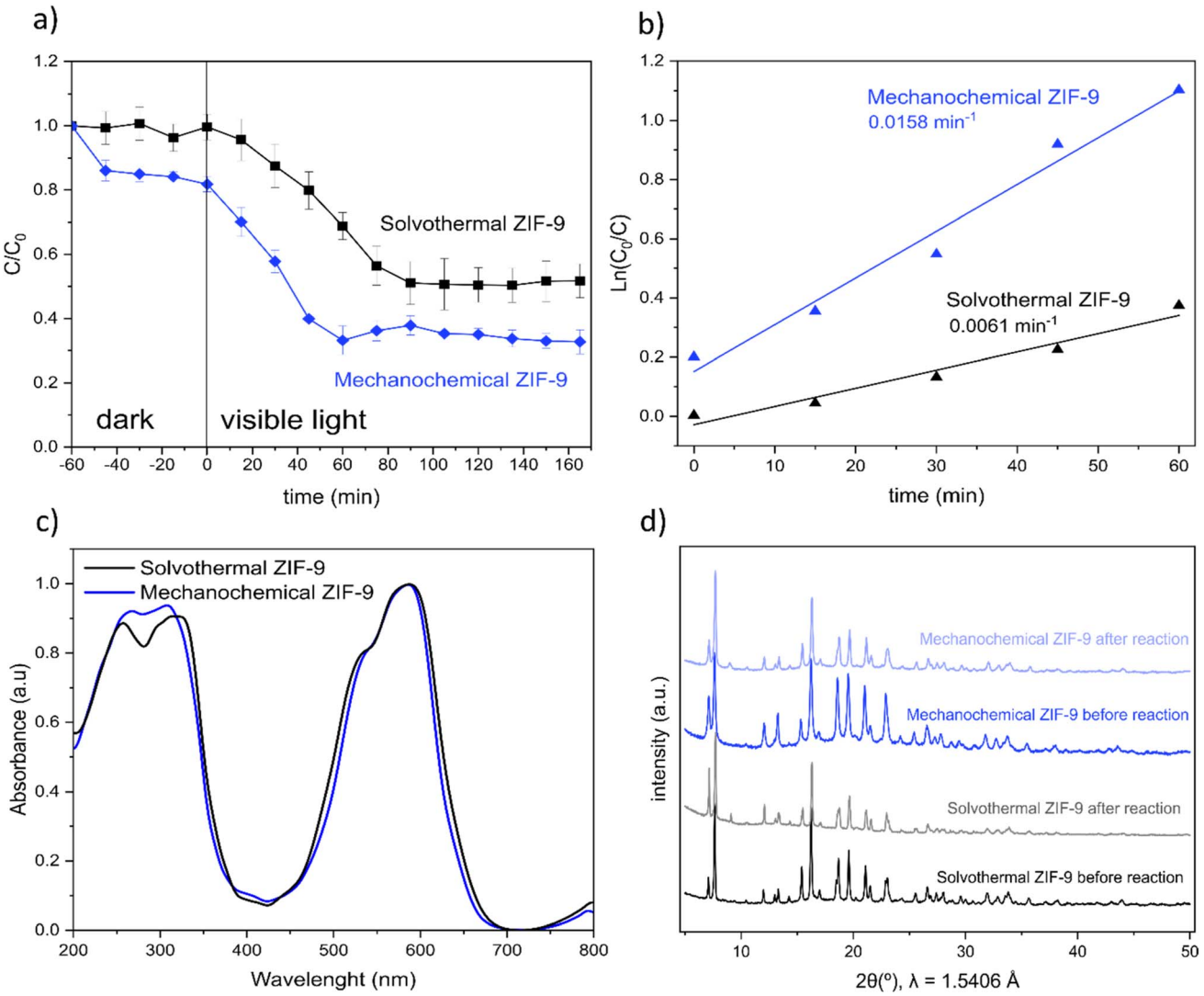

Fig. 5 Degradation of MB by heterogeneous photo-Fenton process using solvothermal synthesized ZIF-9 (■) and mechanochemical synthesized ZIF-9 (◆) as catalyst (a), velocity of MB degradation for solvothermal ZIF-9 (black) and mechanochemical ZIF-9 (blue) (b), UV-vis spectra for solvothermal ZIF-9 (black) and mechanochemical ZIF-9 (blue) (c) and X-ray diffraction patterns for solvothermal ZIF-9 (black) and mechanochemical ZIF-9 (blue) before and after reaction.

9 and 0.0158 min^{-1} for mechanochemical ZIF-9, respectively (Fig. 5b). Zero-order and pseudo-second order kinetics model were also analyzed, being mechanochemical ZIF-9 two times faster in all the adjustments (Fig. S10†). The absence of significant differences in the UV-vis absorption spectra (Fig. 5c), with a maximum absorption peak at 600 nm, suggests that the enhanced photocatalytic performance of mechanochemical ZIF-9 is not due to increased light absorption or band gap reduction. This means that there are rather other factors, such as particle size reduction and plates-shaped particle morphology, that significantly influence the photocatalytic process. The availability of more active sites is crucial to improve the efficiency of charge carrier separation and enhance the interaction between the MOF and the target molecules, which directly contributes to the increased photocatalytic activity.[60] Amano *et al.*, reported similar findings, showing that the increased thickness of platelet-shaped Bi_2WO_6 particles was directly correlated with greater surface area, which in turn was proportional to photocatalytic activity.[61] As previously discussed, TEM images of mechanochemically synthesized ZIF-9 (Fig. 3d and e) suggest the presence of defects. These defects, combined with the high surface area and smaller particle size, can serve as trapping sites for photogenerated electrons and holes, reducing the rate of recombination and thereby prolonging the lifetime of charge carriers and generating more reactive oxygen species (ROS), thus increasing the photocatalytic activity of MOFs.[62] To ensure the accuracy and reproducibility of the results, photo-Fenton assays were repeated three times, resulting in a maximum error of 8% for the tests performed with the solvothermal ZIF-9 and only 2% for the tests performed with the mechanochemically synthesized ZIF-9 (Fig. 5a). XRD analysis of the mechanochemical and solvothermal ZIF-9 after the photo-Fenton tests (Fig. 5d) shows that the overall structure of the ZIFs remains intact, with

characteristic diffraction peaks preserved. While a slight reduction in peak intensity is observed, indicating a minor decrease in crystallinity, the structural integrity is not compromised. Finally, mechanochemical synthetized ZIF-9 was used over three consecutive cycles without significant loss of photocatalytic activity, following a first order kinetic of 0.0158 min^{-1}, 0.0149 min^{-1}, and 0.0142 min^{-1} for cycles 1, 2, and 3, respectively (Fig. S11†). This demonstrates that mechanochemically synthesized ZIFs are as stable as their solvothermal counterparts, making them equally viable for photocatalytic applications, and highlighting their potential for sustainable, efficient catalyst production.

Conclusions

The mechanochemical synthesis of ZIF-9 offers significant advantages over traditional solvothermal methods, particularly in enhancing photocatalytic performance. *In situ* XRD monitoring provided valuable insights into the rapid, one-step reaction mechanism, allowing for optimised synthesis conditions. The mechanochemically prepared ZIF-9 exhibited twice the photocatalytic activity of its solvothermal counterpart, due to higher defect density and smaller particle size. These results highlight mechanochemistry as a promising, sustainable approach for the synthesis of high-performance MOFs. In addition to improving existing properties, this method opens up new avenues for tailoring MOF properties, which is particularly beneficial for applications such as water treatment. Our research highlights the potential of mechanochemical synthesis to advance MOF design and expand their applications in catalysis and environmental remediation, paving the way for further innovation in the field.

Data availability

The data supporting this article have been included as part of the ESI.†

Author contributions

Experimental investigations were carried out by NRS, CP and RB. BB and FE conceived, designed, and supervised the project. NRS prepared the manuscript, which was discussed and agreed by MB, ARR, CP, RB, BB, and FE.

Conflicts of interest

There are no conflicts to declare.

Acknowledgements

The authors thank BESSY II (Helmholtz Zentrum Berlin) for beam time and to Dominik Al-Sabbagh for BESSY data manipulation and computational resources. Also thank to Ines Feldmann for SEM images.

References

1 N. Jorge, A. R. Teixeira, M. S. Lucas and J. A. Peres, Agro-Industrial Wastewater Treatment with Acacia Dealbata Coagulation/Flocculation and Photo-Fenton-Based Processes, *Recycling*, 2022, **7**(4), 54, DOI: 10.3390/recycling7040054.

2 M. S. Mohsen and J. O. Jaber, Potential of Industrial Wastewater Reuse, *Desalination*, 2003, **152**(1–3), 281–289, DOI: 10.1016/S0011-9164(02)01075-5.

3 S. Bauer, H. J. Linke and M. Wagner, Optimizing Water-Reuse and Increasing Water-Saving Potentials by Linking Treated Industrial and Municipal Wastewater for a Sustainable Urban Development, *Water Sci. Technol.*, 2020, **81**(9), 1927–1940, DOI: 10.2166/wst.2020.257.

4 I. Oller and S. Malato, Photo-Fenton Applied to the Removal of Pharmaceutical and Other Pollutants of Emerging Concern, *Curr. Opin. Green Sustainable Chem.*, 2021, **29**, 100458, DOI: 10.1016/j.cogsc.2021.100458.

5 M. Biel-Maeso, C. Corada-Fernández and P. A. Lara-Martín, Removal of Personal Care Products (PCPs) in Wastewater and Sludge Treatment and Their Occurrence in Receiving Soils, *Water Res.*, 2019, **150**, 129–139, DOI: 10.1016/j.watres.2018.11.045.

6 M. Gardner, S. Comber, M. D. Scrimshaw, E. Cartmell, J. Lester and B. Ellor, The Significance of Hazardous Chemicals in Wastewater Treatment Works Effluents, *Sci. Total Environ.*, 2012, **437**, 363–372, DOI: 10.1016/j.scitotenv.2012.07.086.

7 S. Ondrušová, D. Bůžek, M. Kloda, J. Rohlíček, S. Adamec, M. Pospíšil, P. Janoš, J. Demel and J. Hynek, Linker-Functionalized Phosphinate Metal–Organic Frameworks: Adsorbents for the Removal of Emerging Pollutants, *Inorg. Chem.*, 2023, **62**(38), 15479–15489, DOI: 10.1021/acs.inorgchem.3c01810.

8 G. Maniakova, K. Kowalska, S. Murgolo, G. Mascolo, G. Libralato, G. Lofrano, O. Sacco, M. Guida and L. Rizzo, Comparison between Heterogeneous and Homogeneous Solar Driven Advanced Oxidation Processes for Urban Wastewater Treatment: Pharmaceuticals Removal and Toxicity, *Sep. Purif. Technol.*, 2020, **236**, 116249, DOI: 10.1016/j.seppur.2019.116249.

9 M. Muruganandham, R. P. S. Suri, Sh. Jafari, M. Sillanpää, G.-J. Lee, J. J. Wu and M. Swaminathan, Recent Developments in Homogeneous Advanced Oxidation Processes for Water and Wastewater Treatment, *Int. J. Photoenergy*, 2014, **2014**, 1–21, DOI: 10.1155/2014/821674.

10 L. Clarizia, D. Russo, I. Di Somma, R. Marotta and R. Andreozzi, Homogeneous Photo-Fenton Processes at near Neutral pH: A Review, *Appl. Catal., B*, 2017, **209**, 358–371, DOI: 10.1016/j.apcatb.2017.03.011.

11 C. D. Gamarra-Güere, D. Dionisio, G. O. S. Santos, M. R. Vasconcelos Lanza and A. De Jesus Motheo, Application of Fenton, Photo-Fenton and Electro-Fenton Processes for the Methylparaben Degradation: A Comparative Study, *J. Environ. Chem. Eng.*, 2022, **10**(1), 106992, DOI: 10.1016/j.jece.2021.106992.

12 A. Dhakshinamoorthy, A. M. Asiri and H. Garcia, 2D Metal–Organic Frameworks as Multifunctional Materials in Heterogeneous Catalysis and Electro/Photocatalysis, *Adv. Mater.*, 2019, **31**(41), 1900617, DOI: **10.1002/adma.201900617**.

13 J. Demel, P. Kubát, F. Millange, J. Marrot, I. Císařová and K. Lang, Lanthanide-Porphyrin Hybrids: From Layered Structures to Metal–Organic Frameworks with Photophysical Properties, *Inorg. Chem.*, 2013, **52**(5), 2779–2786, DOI: **10.1021/ic400182u**.

14 J. John, K. Ramesh and P. Velayudhaperumal Chellam, Metal–Organic Frameworks (MOFs) as a Catalyst for Advanced Oxidation Processes—Micropollutant Removal, in *Advanced Materials for Sustainable Environmental Remediation*, Elsevier, 2022, pp. 155–174, DOI: **10.1016/B978-0-323-90485-8.00019-9**.

15 M. Cheng, C. Lai, Y. Liu, G. Zeng, D. Huang, C. Zhang, L. Qin, L. Hu, C. Zhou and W. Xiong, Metal-Organic Frameworks for Highly Efficient Heterogeneous Fenton-like Catalysis, *Coord. Chem. Rev.*, 2018, **368**, 80–92, DOI: **10.1016/j.ccr.2018.04.012**.

16 M. Taddei, G. M. Schukraft, M. E. A. Warwick, D. Tiana, M. J. McPherson, D. R. Jones and C. Petit, Band Gap Modulation in Zirconium-Based Metal–Organic Frameworks by Defect Engineering, *J. Mater. Chem. A*, 2019, **7**(41), 23781–23786, DOI: **10.1039/C9TA05216J**.

17 S. L. James, C. J. Adams, C. Bolm, D. Braga, P. Collier, T. Friščić, F. Grepioni, K. D. M. Harris, G. Hyett, W. Jones, A. Krebs, J. Mack, L. Maini, A. G. Orpen, I. P. Parkin, W. C. Shearouse, J. W. Steed and D. C. Waddell, Mechanochemistry: Opportunities for New and Cleaner Synthesis, *Chem. Soc. Rev.*, 2012, **41**(1), 413–447, DOI: **10.1039/C1CS15171A**.

18 S. Kumar, S. Jain, M. Nehra, N. Dilbaghi, G. Marrazza and K.-H. Kim, Green Synthesis of Metal–Organic Frameworks: A State-of-the-Art Review of Potential Environmental and Medical Applications, *Coord. Chem. Rev.*, 2020, **420**, 213407, DOI: **10.1016/j.ccr.2020.213407**.

19 C. Capello, U. Fischer and K. Hungerbühler, What Is a Green Solvent? A Comprehensive Framework for the Environmental Assessment of Solvents, *Green Chem.*, 2007, **9**(9), 927, DOI: **10.1039/b617536h**.

20 J. Chen, K. Shen and Y. Li, Greening the Processes of Metal–Organic Framework Synthesis and Their Use in Sustainable Catalysis, *ChemSusChem*, 2017, **10**(16), 3165–3187, DOI: **10.1002/cssc.201700748**.

21 P. A. Julien, C. Mottillo and T. Friščić, Metal–Organic Frameworks Meet Scalable and Sustainable Synthesis, *Green Chem.*, 2017, **19**(12), 2729–2747, DOI: **10.1039/C7GC01078H**.

22 S. Quaresma, V. André, A. Fernandes and M. T. Duarte, Mechanochemistry – A Green Synthetic Methodology Leading to Metallodrugs, Metallopharmaceuticals and Bio-Inspired Metal-Organic Frameworks, *Inorg. Chim. Acta*, 2017, **455**, 309–318, DOI: **10.1016/j.ica.2016.09.033**.

23 S. J. I. Shearan, N. Stock, F. Emmerling, J. Demel, P. A. Wright, K. D. Demadis, M. Vassaki, F. Costantino, R. Vivani, S. Sallard, I. Ruiz Salcedo, A. Cabeza and M. Taddei, New Directions in Metal Phosphonate and Phosphinate Chemistry, *Crystals*, 2019, **9**(5), 270, DOI: **10.3390/cryst9050270**.

24 G. Ayoub, B. Karadeniz, A. J. Howarth, O. K. Farha, I. Đilović, L. S. Germann, R. E. Dinnebier, K. Užarević and T. Friščić, Rational Synthesis of Mixed-Metal Microporous Metal–Organic Frameworks with Controlled Composition Using Mechanochemistry, *Chem. Mater.*, 2019, **31**(15), 5494–5501, DOI: **10.1021/acs.chemmater.9b01068**.

25 T. Friščić, C. Mottillo and H. M. Titi, Mechanochemistry for Synthesis, *Angew. Chem.*, 2020, **132**(3), 1030–1041, DOI: **10.1002/ange.201906755**.

26 E. Y. Chen, R. M. Mandel and P. J. Milner, Evaluating Solvothermal and Mechanochemical Routes towards the Metal–Organic Framework Mg_2 (*m*-Dobdc), *CrystEngComm*, 2022, **24**(41), 7292–7297, DOI: **10.1039/D2CE00739H**.

27 K. Užarević, I. Halasz and T. Friščić, Real-Time and In Situ Monitoring of Mechanochemical Reactions: A New Playground for All Chemists, *J. Phys. Chem. Lett.*, 2015, **6**(20), 4129–4140, DOI: **10.1021/acs.jpclett.5b01837**.

28 P. F. M. De Oliveira, A. A. L. Michalchuk, A. G. Buzanich, R. Bienert, R. M. Torresi, P. H. C. Camargo and F. Emmerling, Tandem X-Ray Absorption Spectroscopy and Scattering for *In Situ* Time-Resolved Monitoring of Gold Nanoparticle Mechanosynthesis, *Chem. Commun.*, 2020, **56**(71), 10329–10332, DOI: **10.1039/D0CC03862H**.

29 T. Friščić, I. Halasz, P. J. Beldon, A. M. Belenguer, F. Adams, S. A. J. Kimber, V. Honkimäki and R. E. Dinnebier, Real-Time and In Situ Monitoring of Mechanochemical Milling Reactions, *Nat. Chem.*, 2013, **5**(1), 66–73, DOI: **10.1038/nchem.1505**.

30 I. Brekalo, W. Yuan, C. Mottillo, Y. Lu, Y. Zhang, J. Casaban, K. T. Holman, S. L. James, F. Duarte, P. A. Williams, K. D. M. Harris and T. Friščić, Manometric Real-Time Studies of the Mechanochemical Synthesis of Zeolitic Imidazolate Frameworks, *Chem. Sci.*, 2020, **11**(8), 2141–2147, DOI: **10.1039/C9SC05514B**.

31 L. Batzdorf, F. Fischer, M. Wilke, K. Wenzel and F. Emmerling, Direct In Situ Investigation of Milling Reactions Using Combined X-ray Diffraction and Raman Spectroscopy, *Angew. Chem.*, 2015, **127**(6), 1819–1822, DOI: **10.1002/ange.201409834**.

32 S. Darwish, S.-Q. Wang, D. M. Croker, G. M. Walker and M. J. Zaworotko, Comparison of Mechanochemistry vs Solution Methods for Synthesis of 4,4′-Bipyridine-Based Coordination Polymers, *ACS Sustain. Chem. Eng.*, 2019, **7**(24), 19505–19512, DOI: **10.1021/acssuschemeng.9b04552**.

33 M. Campanelli, T. Del Giacco, F. De Angelis, E. Mosconi, M. Taddei, F. Marmottini, R. D'Amato and F. Costantino, Solvent-Free Synthetic Route for Cerium(IV) Metal–Organic Frameworks with UiO-66 Architecture and Their Photocatalytic Applications, *ACS Appl. Mater. Interfaces*, 2019, **11**(48), 45031–45037, DOI: **10.1021/acsami.9b13730**.

34 S. Głowniak, B. Szczęśniak, J. Choma and M. Jaroniec, Mechanochemistry: Toward Green Synthesis of Metal–Organic Frameworks, *Mater. Today*, 2021, **46**, 109–124, DOI: **10.1016/j.mattod.2021.01.008**.

35 T. Friščić, D. G. Reid, I. Halasz, R. S. Stein, R. E. Dinnebier and M. J. Duer, Ion- and Liquid-Assisted Grinding: Improved Mechanochemical Synthesis of Metal–Organic Frameworks Reveals Salt Inclusion and Anion Templating, *Angew. Chem., Int. Ed.*, 2010, **49**(4), 712–715, DOI: **10.1002/anie.200906583**.

36 V. André, S. Quaresma, J. L. F. Da Silva and M. T. Duarte, Exploring Mechanochemistry to Turn Organic Bio-Relevant Molecules into Metal-Organic Frameworks: A Short Review, *Beilstein J. Org. Chem.*, 2017, **13**, 2416–2427, DOI: **10.3762/bjoc.13.239**.

37 S. R. Tavares, N. Ramsahye, G. Maurin and A. A. Leitão, Computational Exploration of the Structure, Stability and Adsorption Properties of the ZIF-9 Metal-Organic Framework, *Microporous Mesoporous Mater.*, 2017, **254**, 170–177, DOI: **10.1016/j.micromeso.2017.05.008**.

38 A. A. L. Michalchuk, E. V. Boldyreva, A. M. Belenguer, F. Emmerling and V. V. Boldyrev, Tribochemistry, Mechanical Alloying, Mechanochemistry: What Is in a Name?, *Front. Chem.*, 2021, **9**, 685789, DOI: **10.3389/fchem.2021.685789**.

39 K. V. Kumar, K. Porkodi and F. Rocha, Langmuir–Hinshelwood Kinetics – A Theoretical Study, *Catal. Commun.*, 2008, **9**(1), 82–84, DOI: **10.1016/j.catcom.2007.05.019**.

40 R. Abazari, A. R. Mahjoub and J. Shariati, Synthesis of a Nanostructured Pillar MOF with High Adsorption Capacity towards Antibiotics Pollutants from Aqueous Solution, *J. Hazard. Mater.*, 2019, **366**, 439–451, DOI: **10.1016/j.jhazmat.2018.12.030**.

41 Q. Song, Y. Fang, Z. Liu, L. Li, Y. Wang, J. Liang, Y. Huang, J. Lin, L. Hu, J. Zhang and C. Tang, The Performance of Porous Hexagonal BN in High Adsorption Capacity towards Antibiotics Pollutants from Aqueous Solution, *Chem. Eng. J.*, 2017, **325**, 71–79, DOI: **10.1016/j.cej.2017.05.057**.

42 K. S. Park, Z. Ni, A. P. Côté, J. Y. Choi, R. Huang, F. J. Uribe-Romo, H. K. Chae, M. O'Keeffe and O. M. Yaghi, Exceptional Chemical and Thermal Stability of Zeolitic Imidazolate Frameworks, *Proc. Natl. Acad. Sci. U. S. A.*, 2006, **103**(27), 10186–10191, DOI: **10.1073/pnas.0602439103**.

43 Z. Öztürk, J. P. Hofmann, M. Lutz, M. Mazaj, N. Z. Logar and B. M. Weckhuysen, Controlled Synthesis of Phase-Pure Zeolitic Imidazolate Framework Co-ZIF-9, *Eur. J. Inorg. Chem.*, 2015, **2015**(9), 1625–1630, DOI: **10.1002/ejic.201403077**.

44 C. Cuadrado-Collados, J. Fernández-Català, F. Fauth, Y. Q. Cheng, L. L. Daemen, A. J. Ramirez-Cuesta and J. Silvestre-Albero, Understanding the Breathing Phenomena in Nano-ZIF-7 upon Gas Adsorption, *J. Mater. Chem. A*, 2017, **5**(39), 20938–20946, DOI: **10.1039/C7TA05922A**.

45 A. Noguera-Díaz, J. Villarroel-Rocha, V. P. Ting, N. Bimbo, K. Sapag and T. J. Mays, Flexible ZIFs: Probing Guest-induced Flexibility with CO_2, N_2 and Ar Adsorption, *J. Chem. Technol. Biotechnol.*, 2019, **94**(12), 3787–3792, DOI: **10.1002/jctb.5947**.

46 Y. Sun, M. Xie, H. Feng and H. Liu, Efficient Visible-Light-Driven Photocatalytic Hydrogen Generation over 2D/2D Co-ZIF-9/Ti_3C_2 Hybrids, *ChemPlusChem*, 2022, **87**(4), e202100553, DOI: **10.1002/cplu.202100553**.

47 F. Afshariazar and A. Morsali, The Unique Opportunities of Mechanosynthesis in Green and Scalable Fabrication of Metal–Organic Frameworks, *J. Mater. Chem. A*, 2022, **10**(29), 15332–15369, DOI: **10.1039/D2TA02699F**.

48 S. Bendt, M. Hovestadt, U. Böhme, C. Paula, M. Döpken, M. Hartmann and F. J. Keil, Olefin/Paraffin Separation Potential of ZIF-9 and ZIF-71: A Combined Experimental and Theoretical Study, *Eur. J. Inorg. Chem.*, 2016, **2016**(27), 4440–4449, DOI: **10.1002/ejic.201600695**.

49 P. Atchutha Rao, H. Padhy, A. Venkateswara Rao, R. Kumar Ganta, S. Bevara, S. Maddila and S. Babu Mukkamala, Facile Synthesis of Benzimidazole Based Mono- and Bimetallic Zeolitic Imidazole Frameworks for Enhanced CO_2 Capture Performance, *Inorg. Chem. Commun.*, 2024, **165**, 112576, DOI: **10.1016/j.inoche.2024.112576**.

50 A. G. Zavyalova, D. V. Kladko, I. Yu. Chernyshov and V. V. Vinogradov, Large MOFs: Synthesis Strategies and Applications Where Size Matters, *J. Mater. Chem. A*, 2021, **9**(45), 25258–25271, DOI: **10.1039/D1TA05283G**.

51 D. Braga, S. L. Giaffreda, F. Grepioni, A. Pettersen, L. Maini, M. Curzi and M. Polito, Mechanochemical Preparation of Molecular and Supramolecular Organometallic Materials and Coordination Networks, *Dalton Trans.*, 2006, **10**, 1249, DOI: **10.1039/b516165g**.

52 P. F. M. De Oliveira, R. M. Torresi, F. Emmerling and P. H. C. Camargo, Challenges and Opportunities in the Bottom-up Mechanochemical Synthesis of Noble Metal Nanoparticles, *J. Mater. Chem. A*, 2020, **8**(32), 16114–16141, DOI: **10.1039/D0TA05183G**.

53 D. Lv, Y. Chen, Y. Li, R. Shi, H. Wu, X. Sun, J. Xiao, H. Xi, Q. Xia and Z. Li, Efficient Mechanochemical Synthesis of MOF-5 for Linear Alkanes Adsorption, *J. Chem. Eng. Data*, 2017, **62**(7), 2030–2036, DOI: **10.1021/acs.jced.7b00049**.

54 A. C. Dodd, A. J. McKinley, M. Saunders and T. Tsuzuki, Effect of Particle Size on the Photocatalytic Activity of Nanoparticulate Zinc Oxide, *J. Nanopart. Res.*, 2006, **8**(1), 43–51, DOI: **10.1007/s11051-005-5131-z**.

55 I. Groeneveld, M. Kanelli, F. Ariese and M. R. Van Bommel, Parameters That Affect the Photodegradation of Dyes and Pigments in Solution and on Substrate – An Overview, *Dyes Pigm.*, 2023, **210**, 110999, DOI: **10.1016/j.dyepig.2022.110999**.

56 A. Peter, A. Mihaly-Cozmuta, C. Nicula, L. Mihaly-Cozmuta, A. Jastrzębska, A. Olszyna and L. Baia, UV Light-Assisted Degradation of Methyl Orange, Methylene Blue, Phenol, Salicylic Acid, and Rhodamine B: Photolysis Versus Photocatalyis, *Water, Air, Soil Pollut.*, 2017, **228**(1), 41, DOI: **10.1007/s11270-016-3226-z**.

57 Y. Zhang, J. Zhou, Q. Feng, X. Chen and Z. Hu, Visible Light Photocatalytic Degradation of MB Using UiO-66/g-C3N4 Heterojunction Nanocatalyst, *Chemosphere*, 2018, **212**, 523–532, DOI: **10.1016/j.chemosphere.2018.08.117**.

58 M. Taheri, I. D. Bernardo, A. Lowe, D. R. Nisbet and T. Tsuzuki, Green Full Conversion of ZnO Nanopowders to Well-Dispersed Zeolitic Imidazolate Framework-8 (ZIF-8) Nanopowders via a Stoichiometric Mechanochemical Reaction for Fast Dye Adsorption, *Cryst. Growth Des.*, 2020, **20**(4), 2761–2773, DOI: **10.1021/acs.cgd.0c00129**.

59 Y. Chen, L. Soler, C. Xie, X. Vendrell, J. Serafin, D. Crespo and J. Llorca, A Straight Forward Method to Prepare Supported Au Clusters by Mechanochemistry and Its Application in Photocatalysis, *Appl. Mater. Today*, 2020, **21**, 100873, DOI: **10.1016/j.apmt.2020.100873**.

60 R. Marschall, Semiconductor Composites: Strategies for Enhancing Charge Carrier Separation to Improve Photocatalytic Activity, *Adv. Funct. Mater.*, 2014, **24**(17), 2421–2440, DOI: **10.1002/adfm.201303214**.

61 F. Amano, K. Nogami, M. Tanaka and B. Ohtani, Correlation between Surface Area and Photocatalytic Activity for Acetaldehyde Decomposition over Bismuth Tungstate Particles with a Hierarchical Structure, *Langmuir*, 2010, **26**(10), 7174–7180, DOI: **10.1021/la904274c**.

62 Z. Zhang, C.-C. Wang, R. Zakaria and J. Y. Ying, Role of Particle Size in Nanocrystalline TiO_2-Based Photocatalysts, *J. Phys. Chem. B*, 1998, **102**(52), 10871–10878, DOI: **10.1021/jp982948+**.